A&A 444, L57–L60 (2005)
DOI: 10.1051/0004-6361:200500211

Astronomy & Astrophysics

Spitzer's large CO_2 ice detection toward the L723 class 0 object⋆

E. Dartois[1], K. Pontoppidan[2], W.-F. Thi[3], and G. M. Muñoz Caro[4]

[1] Institut d'Astrophysique Spatiale, UMR 8617, Université Paris-Sud, bâtiment 121, 91405 Orsay, France
e-mail: emmanuel.dartois@ias.u-psud.fr
[2] Leiden Observatory, PO Box 9513, 2300 RA Leiden, The Netherlands
[3] ESTEC, ESA, Research Support Science Department, PO Box 2200AZ, Noordwijk, The Netherlands
[4] Centro de Astrobiologia, Spain

Received 15 August 2005 / Accepted 3 November 2005

ABSTRACT

The L723 low mass class 0 protostellar object has been observed with the IRS low resolution spectrometer onboard Spitzer Space Telescope. A huge CO_2 ice column density of $6.3 \pm 1 \times 10^{18}$ cm^{-2} is detected toward this extremely red object. We constructed the spectral energy distribution (SED) of L723 by combining the Spitzer spectral data with Infrared Space Observatory (ISO) camera extracted fluxes, IRAS points, ISO long wavelength spectrometer (LWS) observations and millimeter ground based observations. A self consistent 1D model was developed to fit the SED. We show that, besides the high CO_2 column density, the abundance ratio of CO_2 ice to silicates grain cores is similar to other lines-of-sight.

Key words. astrochemistry – line: identification – ISM: dust, extinction – ISM: molecules – ISM: lines and bands – ISM: individual: L723

1. Introduction

L723 is an isolated dark cloud located at a distance of about 300 pc (Goldsmith et al. 1984). It displays a quadrupolar outflow of several arcminutes on the sky, associated with the class 0 source IRAS 19156 + 1906 (Lee et al. 2002, and reference therein). VLA observations revealed a double source (Anglada et al. 1991) named VLA1 and VLA2. The second one is associated with the observed dust millimeter emission (Cabrit & Andre 1991). The bolometric luminosity associated with the object is estimated between about 1.9 $L_\odot$ (Reipurth et al. 1993) to 3.3 $L_\odot$ (Shirley et al. 2000). The highest extinction is confirmed to be associated to VLA2 by CS observations delineating the dense core condensation (Hirano et al. 1998) of about 0.04 pc extension ($\sim 10^4$ AU), with about one solar mass in the circumstellar dust (Estalella et al. 2003). In this paper we present spectroscopic data in the 14–27 μm wavelength range obtained with the Spitzer telescope and showing the presence of large amounts of CO_2 ice. These observations are described in Sect. 2 together with the existing data to build the spectral energy distribution (SED) of this source. We then present the radiative transfer model used to describe the SED in Sect. 3. In the last section we discuss the results and compare the model adopted CO_2 abundance with some of the previous determinations (e.g. de Graauw et al. 1996; Gerakines et al. 1999; Watson et al. 2004; Bergin et al. 2005).

2. Observations

Low-resolution spectra ($R \approx 70$–120) were acquired with the Infrared Spectrograph (IRS, Houck et al. 2004) onboard the Spitzer Space Telescope (Werner et al. 2004) in the Long-Low wavelength acquisition mode, covering the 14–27 μm range. The integration times of the ramps were set to 30 s. Data were reduced at the PBCD level with in-house software extraction using the pipeline calibration files. The distortion of the spectrum on the sky was corrected by fitting a second order polynomial to the trace of the PSF on the wavelength axis, to follow its evolution. The spectrum was extracted with a Gaussian PSF profile weighting scheme centered on this estimated trace. An estimation of the background emission on each side of the point source was subtracted to the spectrum to limit residual contamination. The absolute flux calibration was estimated using the electron-to-Jy conversion polynomial given in the appropriate Spitzer calibration file. The corresponding spectra are displayed in Fig. 1. Additional observations from the literature or database archive were added to produce a spectral energy distribution (SED) overview. The 1.3 mm flux was obtained from Motte & André (2001), the 450 and 850 μm observations from Shirley et al. (2000). In addition to the IRAS fluxes at 25, 60 and 100 μm (the 12 μm is only an upper limit), we added the Infrared Space Observatory LWS spectrometer observations

⋆ This work is based on observations made with the Spitzer Space Telescope (GO-3336 program), which is operated by the Jet Propulsion Laboratory, California Institute of Technology under NASA contract 1407.

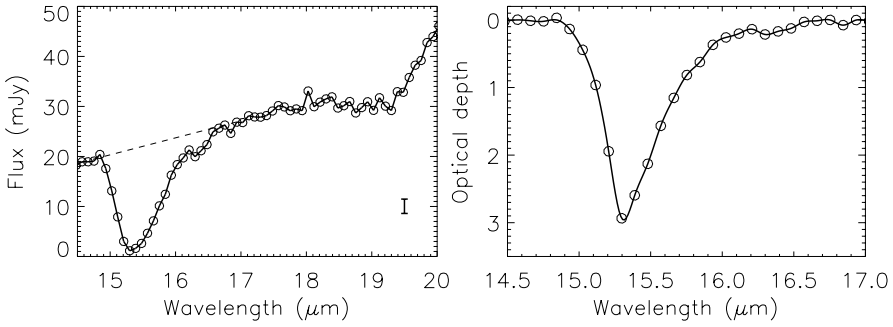

Fig. 1. *Left*: Spitzer IRS observations of IRAS 19156 + 1906 (L723-VLA2) in the 14–27 μm range (see text for details). The deep absorption centered at 15.2 μm arises from the bending mode absorption of CO_2 ice present in the grain mantles. The dashed line represents the expected continuum in the absence of the ice feature. *Right*: extracted optical depth profile of the CO_2 ice bending mode, using the local continuum shown in the left panel, heavily saturated.

Table 1. Summary of observations.

Wavelength (μm)	Flux (Jy)	σ	Bandpass	Ref.
1.25	7.637(−3)	0.153(−3)	1.15–1.35	[a]
1.65	10.730(−3)	0.206(−3)	1.52–1.78	[a]
2.20	9.340(−3)	0.187(−3)	2.03–2.30	[a]
7.75	6.668(−3)	0.636(−3)	7–8.5	[c]
25	0.38	0.0304	8–15	[d]
60	6.93	0.6237	45–80	[d]
95	27	2	78–120	[e]
100	20.72	1.6576	80–120	[d]
130	32	4	110–165	[e]
140	23	3	120–155	[e]
144	33	3	110–380	[e]
166	40	4	130–270	[e]
195	35	2	155–280	[e]
450	12.4	3.1	390–510	[f]
850	3.6	0.23	820–920	[f]
1300	0.37	0.09		[g]
36 000	0.0036	0.0003		[h]
60 000	0.0028	0.0003		[h]

[a] 2MASS cat., [b] ISOCAM TDT31602005, [c] ISOCAM LW6 TDT31902010, [d] IRAS Filters, [e] Davidson (1987), [f] Shirley et al. (2000), [g] Motte & André (2001), [h] Anglada et al. (1996).

extracted from the ISO archive[1] and flux corrected with the extended source flux correction given in the ISO-LWS handbook, Sect. 5.9.3. The data of each individual band were rebinned to produce a single point, without additional gain correction. L723 has also been mapped with ISOCAM in the LW6 filter (7.0–8.5 μm). Data were retrieved from the ISO database and reprocessed with an in house software. These additional fluxes are summarized in Table 1.

3. Model

A 1 D ray-tracing iterative self consistent code based on the moment method has been built to calculate the emergent spectrum of the deeply embedded object. The iterative scheme and temperature correction follows the ones used in e.g. Efstathiou & Rowan-Robinson (1990). The radial density is defined by a power law $n(r(\mathrm{AU})) = n_{100} \times (r(\mathrm{AU})/100\ \mathrm{AU})^{-p}$, where p is the index of the law, r the radial point considered (AU), and n_{100} is the H_2 density at 100 astronomical units (AU). The dust mass equals 1/100th of the H_2 one. The outer radius r_{out} is a fixed input, whereas the inner one (r_{in}) is self consistently determined by the refractory dust sublimation temperature. r_{in} can vary significantly during the first iterations when the opacity is very high. We adopted here a sublimation (destruction) temperature of 1000 K, typical for silicate-like dust particles. Adopting a 500 K inner cavity temperature threshold would not affect the SED output of the model in the observed wavelengths, given the high visual extinction. The constraints on the flux observed in the near infrared for a pure 1D model is hidden by the presence of scattered light probably originating in the outflow cavities walls. The model radial grid contains 50 points equally spaced on a logaritmic scale. 600 angles are considered to evaluate the angular dependent intensity received by a grain at position r. The flux conservacy is estimated by checking the constancy of the moment of second order ($\times r^2$) and the iterations stopped when the value of the standard deviation of the flux conservacy is below 5%, which means a temperature determination to about 1%.

The grains determining the opacity are composed of pure silicates in the region where the evaluated temperature is above ice sublimation (100 K). The location of the ice sublimation front is actualised at each iteration. Where the visual extinction is below a given threshold, we consider bare silicates grains. Such an ice mantle appearance threshold is known for ices since a long time (e.g. Whittet & Duley 1991). We adopt an A_{V} threshold of 3, the minimum expected threshold for the less volatile ices such as H_2O. In the shell delimited by the two above mentioned regions, the grains are coated with an ice mantle whose adopted composition is H_2O:CO_2 (100:15), in agreement with the correlations in many lines of sight (e.g. de Graauw et al. 1996; Gerakines et al. 1999; Watson et al. 2004), with an optimal ice mantle to refractory silicates core volume ratio $V = 1.2$, close to the one expected from the correlation between visual extinction and water ice mantle 3 μm OH stretching mode observations (Dartois 2005, and reference therein). The aim of the study is not to explore the possible detailed ice mantle CO_2 local profile by extracting a local continuum and fitting with pure absorption spectra of laboratory ice films, like presented in Bergin et al. (2005), but rather to make an overall SED ajustment to the observations in order to gain insight into the quantities involved at cloud

[1] http://www.iso.vilspa.esa.es/

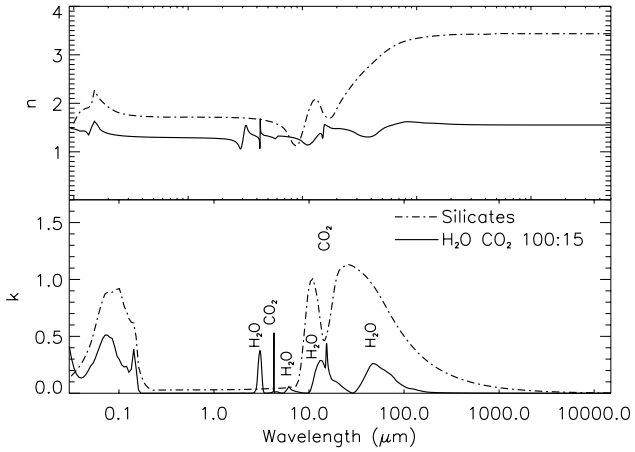

Fig. 2. Absorption and scattering cross-section of the grains. The real (*upper panel*) and imaginary (*lower panel*) part of the complex refractive index of the core interstellar silicates (dot-dashed line) and ice mantle (full line) are displayed. The silicates constants are the Draine & Lee (1984) ones. The H_2O:CO_2 refractive index from 2 to 25 μm was measured at IAS at 10 K. The set was extended using the water dominating mantle absorption measured by Trotta (1996) at wavelengths above 25 μm, and UV-optical data ($\lambda < 2$ μm) were adopted from Warren (1984).

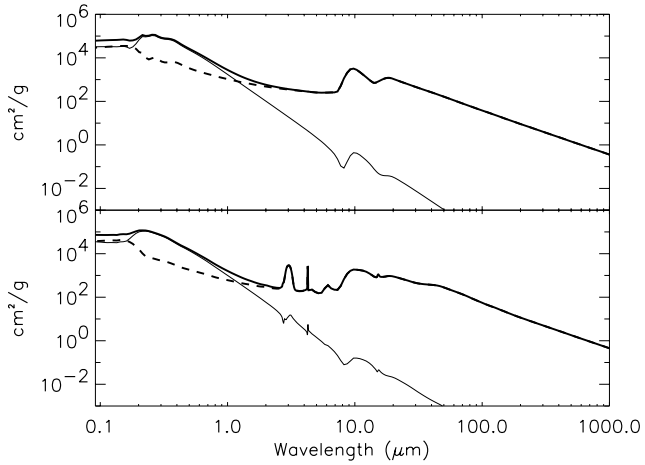

Fig. 3. Mass absorption cross-sections adopted in the radiative transfer model. The dashed line is the absorption, thin one the scattering, and thick line the extinction cross-section. *Upper panel*: silicates ellipsoids with a MRN grain size distribution. *Lower panel*: silicates core/ ice mantle grains with a MRN grain size distribution.

scale. H_2O:CO_2 (2:1) was also tried but revealed to absorb too much in the CO_2 bending mode for such V. The refractive index of the silicates (Draine & Lee 1984) and ice mantle (determined from IAS laboratory transmittance experiments at 10 K, completed by Warren (1984) and Trotta (1996) data, see Fig. 2) were used to calculate the absorption and scattering absorption coefficient, using the Dipole Approximation DDSCAT program. We consider a distribution of randomly oriented ellipsoids with a quadratic shape distribution weighting (like in Fabian et al. 2001) with a mean size of 0.1 μm (i.e. in the Rayleigh limit up to the beginning of the visible). The extinction from the UV to mm calculated for the bare and coated grains are given in Fig. 3.

4. Results

Starting from the best fits obtained in Shirley et al. (2002) and Jorgensen et al. (2002), we explored the $p = 1-2$ parameter space. As described in Shirley et al. (2002) the flux coming from the ISRF in the outer part of the cloud plays an important role for the far infrared flux, as the temperature of the outer part of the envelopes raises or stay constant when approaching the external limit. To take this into account, the temperature in the cloud modelling cannot drop below 15 K, affecting mostly the cloud outer part and can be translated into the ISRF contribution discussed above.

The best fit model is shown in Fig. 4 (corresponding parameters in Table 2), together with the χ^2 minimization surfaces for p indexes of 1., 1.5 and 1.9. These minimizations shown that the best fit is obtained for $p = 1.5$. The best constraint, obtained for the H_2 density at 100 AU, is driven by the Spitzer mid infrared spectrum. The cloud outer radius is much less defined if no additional constraints are put on the model. The physical

Table 2. L723 model's best fit parameters*.

n_{100}	2.2×10^7 cm^{-3}
p	1.5
$r_{\rm out}$	13 400 AU
distance	*300 pc*
$T_{\rm dest}$	*1000 K*
$r_{\rm in}$	0.42 AU (calc. with adopted $T_{\rm dest}$)
$A_{\rm V\ threshold}$	*3*
$M_{\rm cloud}$	1.6 $M_\odot$
$L_{\rm bol}$	3.4 $L_\odot$

* Values in italic are adopted parameters.

extension of the cloud observed by Shirley et al. (2002) favors also the $p \gtrsim 1.5$ case.

The near infrared (NIR) excess observed with 2MASS, and not reproduced in the framework of the 1D model, is due to escaping photons scattered by the walls of the cavity digged by the powerful quadrupolar outflow. Deep images in the K' band confirm that the NIR source is extended (Lee et al. 2002). The NIR observations can be reasonably reproduced with a stellar spectrum reprocessed by dust, as shown in Fig. 4. The scattering efficiency drop radically above $\sim$2 μm, and the remaining flux can be well fitted with a spherical envelope in which is embedded the young source.

The CO_2/H_2O ratio adopted to reproduce the observations is in perfect agreement with the adopted ice to core volume ratio of one, coupled to a CO_2/H_2O ratio of about 15%, numbers compatible with the numerous observations performed with ISO (e.g. Gerakines et al. 1999) and Spitzer (e.g. Watson et al. 2004). However, the water ice features model should be constrained in additional spectral regions. The ice region pencil beam column density, for the best model, represents from $\sim$1/3.3th (500 K sublimation temp.) to $\sim$1/7th (1000 K sublimation temp.) of the inner "ice ree" column density. In volume, the ice region largely dominates over the inner "ice free" one.

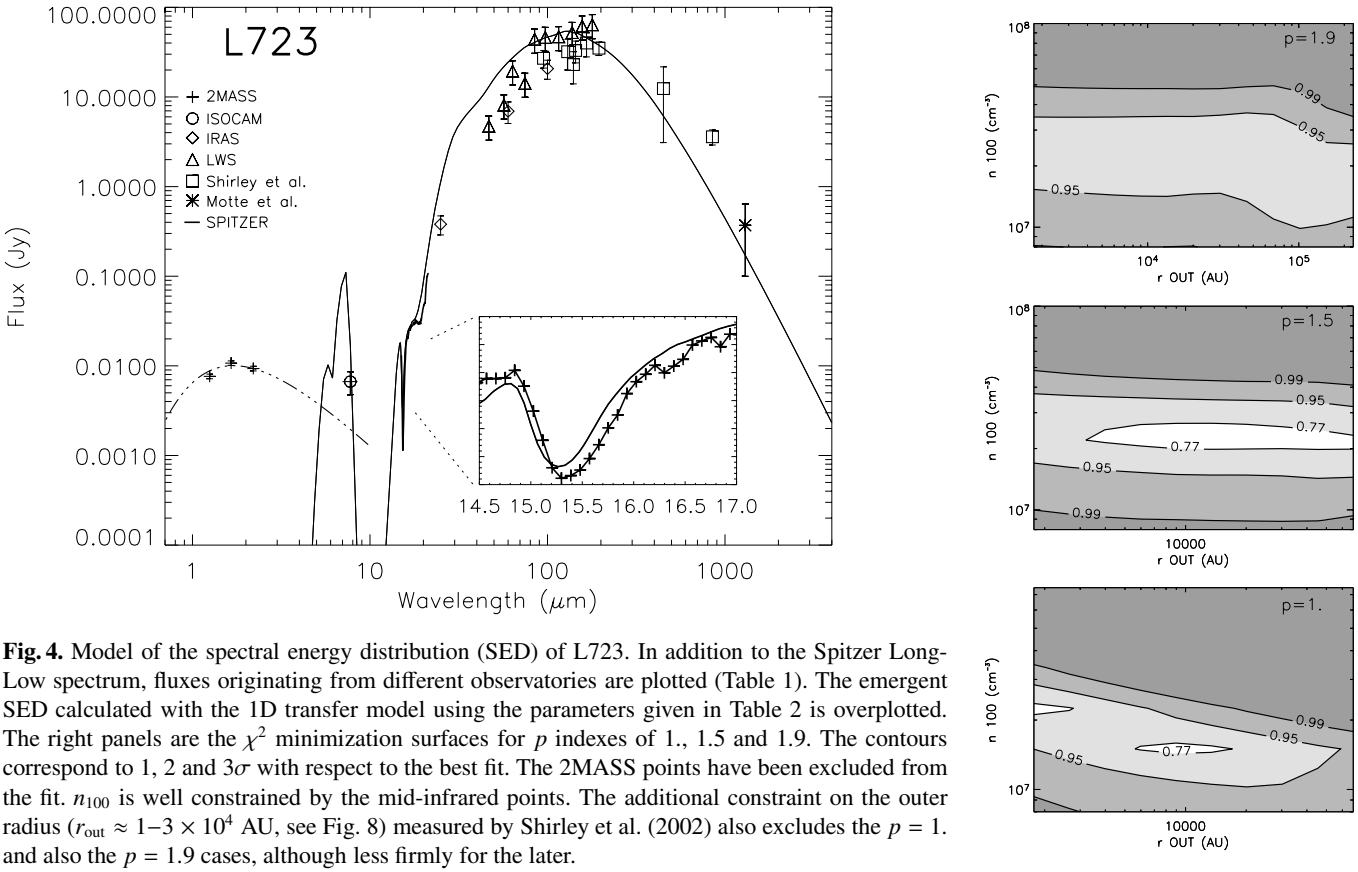

Fig. 4. Model of the spectral energy distribution (SED) of L723. In addition to the Spitzer Long-Low spectrum, fluxes originating from different observatories are plotted (Table 1). The emergent SED calculated with the 1D transfer model using the parameters given in Table 2 is overplotted. The right panels are the χ^2 minimization surfaces for p indexes of 1., 1.5 and 1.9. The contours correspond to 1, 2 and 3σ with respect to the best fit. The 2MASS points have been excluded from the fit. n_{100} is well constrained by the mid-infrared points. The additional constraint on the outer radius ($r_{\rm out} \approx 1{-}3 \times 10^4$ AU, see Fig. 8) measured by Shirley et al. (2002) also excludes the $p = 1.$ and also the $p = 1.9$ cases, although less firmly for the later.

The total pencil beam column density is of the order of $n(H_2, T_{\rm dest} = 500\ {\rm K}) \sim 4.9 \times 10^{23}$ cm^{-2} or $n(H_2, T_{\rm dest} = 1000\ {\rm K}) \sim 1.0 \times 10^{24}$ cm^{-2}). Taking into account only the ice region, locally, $[CO_2]/[H_2] \sim 3.6 \times 10^{-5}$. If effectively $CO_2/H_2O \approx 0.15$ in the ice region, at least 30% of the cosmic available oxygen is locked into the ice mantles.

5. Conclusions

IRAS 19156+1906 in the L723 cloud display a huge quantity of ices along the line of sight, as traced by the Spitzer observations of the CO_2 ice bending mode around 15.2 μm. The estimated column density of $N(CO_2) = 6.3 \pm 1 \times 10^{18}$ cm^{-2} is one of the highest ever detected. The modeling of the complete spectral distribution reveals however that its relative abundance is not much higher than what is expected from the correlations found in other lines of sight. Nontheless it implies that about 30% of the cosmic oxygen is trapped into ice mantles at this stage of the L723 cloud's evolution.

Acknowledgements. W. F. Thi acknowledges an ESA Research Fellowship at ESTEC. We thank A. Abergel for retrieving and reducing the ISOCAM data.

References

Anglada, G., Estalella, R., Rodriguez, L. F., et al. 1991, ApJ, 376, 615
Anglada, G., Rodriguez, L. F., & Torrelles, J. M. 1996, ApJ, 473, L123
Bergin, E. A., Melnick, G. J., Gerakines, P. A., Neufeld, D. A., & Whittet, D. C. B. 2005, ApJ, 627, L33
Cabrit, S., & Andre, P. 1991, ApJ, 379, L25
Dartois, E. 2005, A&A, submitted
Davidson, J. A. 1987, ApJ, 315, 602
Draine, B. T., & Lee, H. M. 1984, ApJ, 285, 89
Efstathiou, A., & Rowan-Robinson, M. 1990, MNRAS, 245, 275
Estalella, R., Palau, A., Girart, J. M., et al. 2003, Rev. Mex. Astron. Astrofis. Conf. Ser., 15, 135
Fabian, D., Henning, T., Jäger, C., et al. 2001, A&A, 378, 228
Gerakines, P. A., Whittet, D. C. B., Ehrenfreund, P., et al. 1999, ApJ, 522, 357
Goldsmith, P. F., Snell, R. L., Hemeon-Heyer, M., & Langer, W. D. 1984, ApJ, 286, 599
de Graauw, T., Whittet, D. C. B., Gerakines, P. A., et al. 1996, A&A, 315, L345
Hirano, N., Hayashi, S. S., Umemoto, T., & Ukita, N. 1998, ApJ, 504, 334
Houck, J. R., Roellig, T. L., van Cleve, J., et al. 2004, ApJS, 154, 18
Jørgensen, J. K., Schöier, F. L., & van Dishoeck, E. F. 2002, A&A, 389, 908
Lee, C., Mundy, L. G., Stone, J. M., & Ostriker, E. C. 2002, ApJ, 576, 294
Motte, F., & André, P. 2001, A&A, 365, 440
Murakawa, K., Tamura, M., & Nagata, T. 2000, ApJS, 128, 603
Reipurth, B., Chini, R., Krugel, E., Kreysa, E., & Sievers, A. 1993, A&A, 273, 221
Shirley, Y. L., Evans, N. J., & Rawlings, J. M. C. 2002, ApJ, 575, 337
Shirley, Y. L., Evans, N. J., Rawlings, J. M. C., & Gregersen, E. M. 2000, ApJS, 131, 249
Trotta, F. 1996, Ph.D. Thesis, Université Joseph Fourier, Grenoble
Warren, S. G. 1984, Appl. Opt., 23, 1206-1225
Watson, D. M., Kemper, F., Calvet, N., et al. 2004, ApJS, 154, 391
Werner, M. W., Roellig, T. L., Low, F. J., et al. 2004, ApJS, 154, 1
Whittet, D. C. B., & Duley, W. W. 1991, A&ARv, 2, 167